

This is the accepted manuscript made available via CHORUS. The article has been published as:

Quaternary phase diagrams of spinel  
 $\text{Li}_{\{y\}}\square_{\{1-y\}}\text{Mn}_{\{x\}}\text{Ni}_{\{2-x\}}\text{O}_{\{4\}}$  and composite  
cathode voltages for concentration gradient materials

Shiqiang Hao, Zhi Lu, and Christopher Wolverton

Phys. Rev. B **94**, 014114 — Published 19 July 2016

DOI: [10.1103/PhysRevB.94.014114](https://doi.org/10.1103/PhysRevB.94.014114)

# Quaternary Phase Diagrams of Spinel $\text{Li}_y\text{□}_{1-y}\text{Mn}_x\text{Ni}_{2-x}\text{O}_4$ and Composite Cathode Voltages for Concentration Gradient Materials

Shiqiang Hao, Zhi Lu, and Christopher Wolverton  
*Department of Materials Science & Engineering,  
Northwestern University, Evanston, Illinois 60208, USA*

## Abstract

Core-shell coating structures and concentration gradient materials may enhance Li ion battery performance by integrating advantages of core and shell components without introducing unfavorable problems associated with general coatings. The fundamental thermodynamic properties of the concentration gradient composite materials are complex due to the multicomponent nature of the problem. We systematically study the thermodynamics of ordering and phase-separation in the quaternary spinel  $\text{Li}_y\text{□}_{1-y}\text{Mn}_x\text{Ni}_{2-x}\text{O}_4$  ( $\square$  means vacancy) system by density functional theory calculations together with the coupled cluster expansion method with interactions within and between (Li/ $\square$ ) and (Mn/Ni) sublattices. On the basis of coupled cluster expansion interactions and Monte Carlo simulations, we calculate quaternary phase diagrams as a function of temperature as well as voltage profiles of single ordered phases and multi-phase composite structures. The phase diagram and voltage results are in good agreement with available experimental observations. We also predict a new, stable high-voltage ordered compound  $\text{LiMnNiO}_4$ , with a very high delithiation voltage of 4.76 V. For the composite (Mn-rich + Ni-rich) cathode materials, the voltage profiles show combinations of plateaus from each component compound. The computational strategy of combining quaternary phase diagrams with voltage calculations provides a pathway to understand and design concentration gradient materials.

PACS numbers: 88.80.ff, 81.30.Bx, 31.15.A-

## I. INTRODUCTION

Lithium-ion batteries possess great advantages for use as large-scale energy storage devices because of higher energy densities and longer operational lifetimes than other rechargeable battery systems.[1–3] However, several failure mechanisms have limited the commercial utilization of many cathode materials, including capacity degradation due to dissolution of redox-active metal into electrolytes, collapse of the structure induced by volume changes during the cycling processes, low mobility of electrons and Li ions, etc. Researchers have proposed various strategies to overcome these troublesome obstacles, such as optimizing the crystalline lattice of active materials by mixing multiple metals, reducing particle size to enhance Li conductivity and reactivity, combining active materials and other active/inactive materials together for complementary performance enhancement, etc. Among the various feasible strategies, surface coating technology is one effective way to improve battery performance.[4, 5]

The coating materials investigated to date include various carbons,[6] metal oxides, [7] metal phosphates, [8] metal fluorides, [9] etc. Many coating materials on the one hand may suppress metal dissolution or provide anti-corrosion properties [10, 11] successfully, however on the other hand, they often introduce other problems such as decreasing Li mobility [12] or discontinuity of volume [13] and hence design and choice of coating materials are difficult, but critical to help improve overall performance.

The strategy of using a concentration-gradient material provides an opportunity to overcome the general problems associated with coatings, [14, 15] since the gradual change of metal concentration reduces the discontinuity of volume when going from active electrode to coating. In concentration gradient materials based on layered lithium transition-metal (TM) oxides, the concentration of one TM decreases gradually whereas the concentration of another TM increases gradually from the core to the shell layer. Hence, both the core and shell materials are active, forming a composite or mixed cathode. For Ni/Mn based layered materials, the concentration-gradient composite material has achieved many advantages including not only the high energy density of the Ni-rich core and high thermal stability of the Mn-rich outer layers, but also superior performance of cyclic stability without decreasing ionic mobility. [14] The successful demonstration of concentration-gradient materials thus opens a new field for cathode development.

In this paper, we focus on the spinel  $\text{Li}_y\text{Mn}_x\text{Ni}_{2-x}\text{O}_4$  system aiming to integrate the advantages of concentration-gradient materials mentioned above with high voltage and rate capabilities offered by the spinel materials. Using a density functional theory derived coupled cluster expansion along with Monte Carlo simulations,[16, 17] we not only predict ordered quaternary phase formation of spinel compounds, such as  $\text{LiMnNiO}_4$ , but also construct a quaternary phase diagrams for this battery material. Also, by investigating voltage curves of composite multi-phase materials, we find the voltages show combinations of plateaus from each spinel component. The fundamental phase diagram information and composite voltage plateaus provide useful information to help design concentration-gradient particles with specified, targeted voltage profiles.

## II. CALCULATIONS

The total energies and relaxed geometries were calculated by density-functional theory (DFT) within the generalized gradient approximation of Perdew-Burke-Ernzerhof for the exchange-correlation functional with Projector Augmented Wave potentials and Hubbard U (GGA+U).[18–20] We use periodic boundary conditions and a plane wave basis set as implemented in the Vienna *ab initio* simulation package.[21] The total energies were numerically converged to approximately 3 meV/cation using a basis set energy cutoff of 500 eV and dense  $k$ -meshes corresponding to 4,000  $k$ -points per reciprocal atom in the Brillouin zone. The Hubbard U parameters for Mn and Ni atoms are  $U-J= 5.00$  and  $5.96$  eV respectively.[22] Even though ferrimagnetic spin arrangements of Mn and Ni are favorable for some materials (such as  $\text{LiMn}_{1.5}\text{Ni}_{0.5}\text{O}_4$ ), the energy differences between ferrimagnetic and ferromagnetic are usually small (0.007 eV/f.u. for  $\text{LiMn}_{1.5}\text{Ni}_{0.5}\text{O}_4$ ). In our case, we use ferromagnetic spins for Mn and Ni ions with initial magnetic moments of  $5 \mu_B$ .

The cluster expansion (CE) approach was used to construct an effective Hamiltonian for energy evaluation on the spinel structure. We used the ATAT toolkit to obtain the optimal effective cluster interactions from fully relaxed total energies of ordered input structures.[23] In a typical simple binary cluster expansion, a spin variable  $\sigma_i$  with a value of  $\pm 1$  denotes the type of atom sitting on each site  $i$ . In a coupled cluster expansion, two interacting lattices can be simultaneously considered with a different set of spin variables for each of the two sublattices ( $\sigma, \theta$ ).[17] Cluster functions are then defined with products of spin

variables from either or both sublattices, [17]  $E(\sigma, \theta) = V_0 + \sum_i V_i \sigma_i + \sum_i V_i \theta_i + \sum_{i,j} V_{i,j} \sigma_i \sigma_j + \sum_{i,j} V_{i,j} \sigma_i \theta_j + \sum_{i,j} V_{i,j} \theta_i \theta_j + \sum_{i,j,k} V_{i,j,k} \sigma_i \sigma_j \theta_k + \sum_{i,j,k} V_{i,j,k} \sigma_i \theta_j \theta_k + \dots$ , where  $V_{i,j,k}$  are effective cluster interactions. For the quaternary system  $\text{Li}_y \square_{1-y} \text{Mn}_x \text{Ni}_{2-x} \text{O}_4$ , the two spin variables describe the arrangement of Li/ $\square$  on Li sites and Mn/Ni on transition metal sites. By fitting 43 ordered input structures, the final cluster expansion contains 11 interaction coefficients, including 3 two-body, 3 three-body and 2 four-body interactions, resulting in a leave-one-out cross-validation score as 8.7 meV/metal, which is only about 5% of the most favorable formation energy of -160 meV. The quaternary formation energy can be defined as  $\Delta H(\sigma) = E_{\text{tot}}(\sigma) - (1-x-y)E_{\text{tot}}^{\text{AC}} - xE_{\text{tot}}^{\text{BC}} - yE_{\text{tot}}^{\text{AD}}$ . Here, AC, BC, and AD are respectively  $\text{LiMn}_2\text{O}_4$ ,  $\square\text{Mn}_2\text{O}_4$ , and  $\text{LiNi}_2\text{O}_4$  with A=Li, B= $\square$ , C= Mn, and D=Ni. Note that  $\Delta H(\sigma)$  is not a true formation energy with respect to elements but is given with respect to binary constituent component. For quasi-binary systems, the formation energy  $\Delta H$  of a  $\text{A}_{1-x}\text{B}_x\text{C}$  with respect to the energies of pure constituents AC and BC can be simplified as  $\Delta H(\sigma) = E_{\text{tot}}(\sigma) - (1-x)E_{\text{tot}}^{\text{AC}} - xE_{\text{tot}}^{\text{BC}}$ , where  $E_{\text{tot}}(\sigma)$ ,  $E_{\text{tot}}^{\text{AC}}$  and  $E_{\text{tot}}^{\text{BC}}$  are total energy of phases  $\text{A}_{1-x}\text{B}_x\text{C}$ , AC and BC, respectively. For example, in the binary case of  $\text{LiMn}_x\text{Ni}_{2-x}\text{O}_4$ , the formation energies of  $\text{LiMn}_x\text{Ni}_{2-x}\text{O}_4$  ( $\text{A}_{1-x}\text{B}_x\text{C}$ ) are calculated with respect to the references of spinel  $\text{LiMn}_2\text{O}_4$  (AC) and spinel  $\text{LiNi}_2\text{O}_4$  (BC).

On the basis of the well-converged effective cluster interactions, the temperature-composition phase diagrams are calculated by semigrand Canonical Monte Carlo simulations.[24] In this semigrand canonical ensemble, the energy and concentrations (x and y) of the system are allowed to fluctuate while temperature and chemical potentials are externally imposed. By scanning over temperature and chemical potentials, the two-phase regions in the phase diagram can be determined from discontinuities of composition as a function of chemical potential. We use a  $40 \times 40 \times 40$  unit cell as a simulation cell, and the simulated temperatures range from 50 to 1500 K with a 50 K interval. We use MC 50000 steps to equilibrate and 100000 steps for averaging, and we monitor the composition change with chemical potential at a given temperature. The thermodynamic state is thus determined as a function of the temperature and the chemical potential differences of the constituents. To check for hysteresis in the phase diagram results, we have repeated Monte Carlo simulations by stepping through chemical potential in both directions. We find no big differences between these two simulations, confirming the accuracy of the phase diagrams.

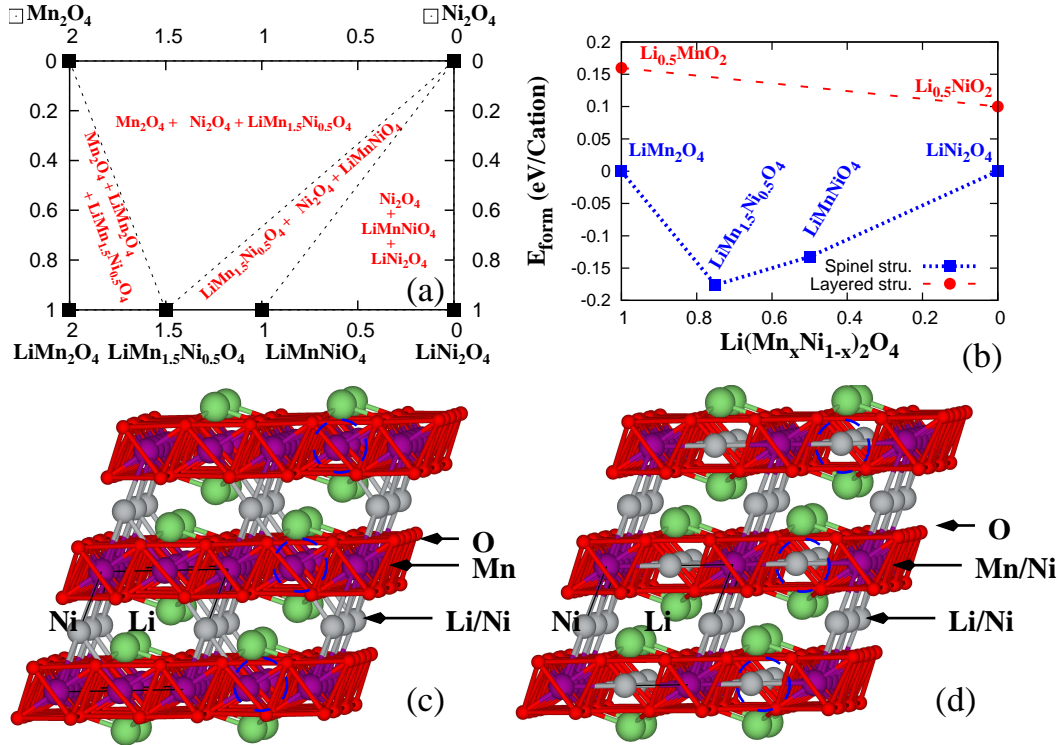


FIG. 1: (a) Quaternary ground state diagram of  $\text{Li}_y\text{Mn}_x\text{Ni}_{2-x}\text{O}_4$  at 0 K. (b) Formation energy comparison of spinel structures with same composition of layered  $\text{Li}_{0.5}\text{MnO}_2$  and  $\text{Li}_{0.5}\text{NiO}_2$ . (c) Atomic structure of spinel  $\text{LiMn}_{1.5}\text{Ni}_{0.5}\text{O}_4$ . (d) Predicted crystal structure of spinel  $\text{LiMnNiO}_4$ . Note that the structure difference between  $\text{LiMn}_{1.5}\text{Ni}_{0.5}\text{O}_4$  and  $\text{LiMnNiO}_4$  is highlighted by blue circles, where metal Mn layer in  $\text{LiMn}_{1.5}\text{Ni}_{0.5}\text{O}_4$  is partially substituted by Ni in  $\text{LiMnNiO}_4$  while keeping other configuration the same.

### III. RESULTS

With the DFT-derived coupled CE combined with Monte Carlo, we predict the stable phases of  $\text{Li}_y\text{Mn}_x\text{Ni}_{2-x}\text{O}_4$  and the formation energy of all 62144 spinel-based ordered structures with less than 42 atoms per unit cell. By constructing a convex hull such that no structure lies below the planes connecting the vertices of this object, we can identify the most favorable ordered spinel structures. On the basis of formation energies, we find that within the constrained space of only considering orderings on the spinel structure, the system prefers Ni/Mn mixing, or compound forming along  $\text{LiMn}_x\text{Ni}_{2-x}\text{O}_4$  since the formation energy of these compounds are negative, hence favorable with respect to spinel  $\text{LiMn}_2\text{O}_4$  and  $\text{LiNi}_2\text{O}_4$ . It is worth mentioning that  $\text{LiMn}_2\text{O}_4$  is observed in the spinel structure while  $\text{LiNi}_2\text{O}_4$  is

not ( $\text{LiNiO}_2$  forms a layered compound), so competition between spinel, layered and other compounds becomes more relevant as one goes from Mn-rich to Ni-rich. The quaternary  $T=0$  K ground state diagram of  $\text{Li}_y\text{Mn}_x\text{Ni}_{2-x}\text{O}_4$  is shown in Fig.1(a). There are two ordered phases at the Li-rich boundary at  $x = 1$  and  $x = 1.5$  corresponding to ordered  $\text{LiMnNiO}_4$  and  $\text{LiMn}_{1.5}\text{Ni}_{0.5}\text{O}_4$  quaternary spinel compounds, respectively. The formation energies of spinel  $\text{LiMn}_x\text{Ni}_{2-x}\text{O}_4$  as a function of  $x$  as shown in Fig.1(b) have been also compared with the partially delithiated layered analogues  $\text{Li}_{0.5}\text{MnO}_2$  and  $\text{Li}_{0.5}\text{NiO}_2$ . Even though the fully lithiated layered  $\text{LiNiO}_2$  is more favorable in energy than spinel  $\text{LiNi}_2\text{O}_4$ , the half delithiated layered  $\text{Li}_{0.5}\text{NiO}_2$  is higher in energy than the corresponding spinel  $\text{LiNi}_2\text{O}_4$ . The spinel  $\text{LiMn}_{1.5}\text{Ni}_{0.5}\text{O}_4$  is a well known experimentally observed compound,[25] and our DFT combined with CE method gives the identical structure to that observed. The  $\text{LiMn}_{1.5}\text{Ni}_{0.5}\text{O}_4$  has primitive simple cubic structure as plotted in Fig.1(c). In the  $[111]$  direction, the metal Mn layers lie between the two layers of oxygen forming MnO blocks, while the Li/Ni layers are intercalated between MnO blocks. Our predicted ordered  $\text{LiMnNiO}_4$  spinel is in the  $\text{Imma}$  space group and is the same structure as previously reported.[26] In this spinel structure as shown in Fig.1(d), the Mn layer between the two oxygen layers is partially substituted by Ni while keeping other layers configuration unchanged.

Beyond the 0 K convex hull, we also investigated the temperature dependence of the quaternary phase diagram. An isothermal section of the quaternary phase diagrams at 300 K is plotted in Fig.2(a), with Ni/Mn concentration ( $x$ ) along the horizontal axis and Li/ $\square$  concentration ( $y$ ) along the vertical axis. The boundaries of the quaternary phase diagram correspond to binary phase diagrams, where only one composition  $x$  or  $y$  in  $\text{Li}_y\text{Mn}_x\text{Ni}_{2-x}\text{O}_4$  is varied and the other is fixed. These binary phase diagrams are shown in Figs.2b-e. For the binary alloying (varying  $x$ ,  $y=1$ ) of  $\text{LiMn}_x\text{Ni}_{2-x}\text{O}_4$  at 300 K, as shown in Fig. 2(e), the phase regions from  $x = 0$  to 2 are respectively solid solution of  $\text{LiNi}_2\text{O}_4$ , two phase coexistence of  $\text{LiNi}_2\text{O}_4$  and  $\text{LiMnNiO}_4$ , single phase of  $\text{LiMnNiO}_4$ , and two phase coexistence of  $\text{LiMnNiO}_4$  and  $\text{LiMn}_{1.5}\text{Ni}_{0.5}\text{O}_4$ , etc. We note two interesting characteristics of the binary phase diagram, the new predicted ordered structure of  $\text{LiMnNiO}_4$  as mentioned above, and the metal off-stoichiometry range  $\delta$  in the single phase of  $\text{LiMn}_{1.5\pm\delta}\text{Ni}_{0.5\mp\delta}\text{O}_4$  is significant. We find an off-stoichiometry of about  $\delta=0.2$  at 700 K, which is consistent with the experimental reports of off-stoichiometric compositions in spinel structures of  $\text{LiMn}_{1.82}\text{Ni}_{0.18}\text{O}_4$ , [27]  $\text{LiMn}_{1.67}\text{Ni}_{0.33}\text{O}_4$  [28] and  $\text{LiMn}_{1.53}\text{Ni}_{0.47}\text{O}_4$ . [28] We also predict an order-disorder tran-

sition of  $\text{LiMn}_{1.5}\text{Ni}_{0.5}\text{O}_4$  into a high-temperature spinel solid solution. Experimentally, it is known that  $\text{LiMn}_{1.5}\text{Ni}_{0.5}\text{O}_4$  samples has undergo a transition from spinel to rock-salt at around  $700^\circ\text{C}$  with an associated oxygen loss.[29] Another experimental investigation on Ni and Mn ordering in  $\text{LiMn}_{1.5}\text{Ni}_{0.5}\text{O}_4$  samples by annealing at  $700^\circ\text{C}$  in air shows that the fraction of rock-salt ordered phase increases rapidly during initial annealing for 6 h, and accompanied by decreasing amounts of secondary phases.[30] These experimental studies involved ordered rock-salt phases with oxygen vacancies (which are not considered here) and suggest that a hypothetical Ni/Mn order-disorder spinel transition temperature should be higher than  $700^\circ\text{C}$ . In our calculations of  $\text{LiMn}_x\text{Ni}_{2-x}\text{O}_4$ , we keep the oxygen amount fixed and stoichiometric for spinel by only considering Mn and Ni interactions and the calculated transition temperature is around 800 K, slightly below the observed rocksalt transformation temperature.

In contrast to  $\text{LiMn}_x\text{Ni}_{2-x}\text{O}_4$ , the fully delithiated binary  $\square\text{Mn}_x\text{Ni}_{2-x}\text{O}_4$  system shows phase separation characterized by a miscibility gap and positive mixing energies relative to pure  $\square\text{Mn}_2\text{O}_4$  and  $\square\text{Ni}_2\text{O}_4$ . Except for the fully delithiated spinel structure of  $\square\text{Mn}_2\text{O}_4$  (often referred as  $\lambda\text{-MnO}_2$ ), there are no stable spinel  $\square\text{Mn}_x\text{Ni}_{2-x}\text{O}_4$  compounds reported experimentally. It is worth mentioning that the stable spinel compound  $\text{NiMn}_2\text{O}_4$  [31] with space group  $\text{Fd}\bar{3}\text{m}$  should not appear in our phase diagrams, because Ni atoms occupy Li sites, rather than mixing with Mn in metal (16d) sites. There are some other stable Mn-Ni-O compounds such as  $\text{Mn}_{0.75}\text{Ni}_{0.25}\text{O}$  ( $\text{Fm}\bar{3}\text{m}$ ), [32]  $\text{MnNi}_6\text{O}_8$  ( $\text{Fm}\bar{3}\text{m}$ ), [33] and  $\text{NiO}_2$  ( $\text{R}\bar{3}\text{m}$ ), but none of them is in spinel structure, thus not shown in our phase diagrams. The boundaries of the quaternary phase diagram in Fig. 2(a) on the Mn-rich and Ni-rich edges reflect the (de)lithiation process of  $\text{Li}_y\text{Mn}_2\text{O}_4$  and  $\text{Li}_y\text{Ni}_2\text{O}_4$ , respectively. The phase diagrams of these two cases are both phase separation reflected as miscibility gaps. Note that for the different Hubbard  $U$  values for Mn from 0 to 6 eV, our calculated formation energy of  $\text{Li}_{0.5}\text{Mn}_2\text{O}_4$  (relative to  $\text{LiMn}_2\text{O}_4 + \text{Mn}_2\text{O}_4$ ) ranges from -0.15 to 0.12 eV/f.u., suggesting that the binary phase diagram of  $\text{Li}_y\text{Mn}_2\text{O}_4$  shifts from phase separation (for  $U > 2$  eV) to Li/ $\square$  ordering, or compound formation (for  $U \leq 1$  eV). These results agree with previous calculations where Li ordering was found in  $\text{Li}_y\text{Mn}_2\text{O}_4$  with  $U=0$  eV [34] and phase separation with  $U = 5.00$  eV.[35] Even though an ordered  $\text{Li}_{0.5}\text{Mn}_2\text{O}_4$  phase has been proposed to reflect the step in the discharge potential curve,[36] neutron studies showed no evidence of the ordered structure formation.[37] There are no experimental results to

compare with for our spinel-based  $\text{Li}_y\text{Ni}_2\text{O}_4$  phase diagram.

Our calculated phase diagram provides useful information to understand and design the structure of concentration-gradient materials on the basis of the binary phase diagram of  $\text{LiMn}_x\text{Ni}_{2-x}\text{O}_4$ . For example, to grow a core-shell type concentration-gradient material with a spinel  $\text{LiMn}_2\text{O}_4$  core and spinel Ni-rich shell, by gradually increase Ni concentration, the thermodynamic stable structures from core to shell should be  $\text{LiMn}_2\text{O}_4$ ,  $\text{LiMn}_{1.5}\text{Ni}_{0.5}\text{O}_4$ ,  $\text{LiMnNiO}_4$ , and  $\text{LiNi}_2\text{O}_4$ . The intermediate structures are the single phases as shown in Fig.2(e). On the contrary, for a core-shell type material with a  $\square\text{Mn}_2\text{O}_4$  core and  $\square\text{Ni}_2\text{O}_4$  shell, there should not be any intermediate thermodynamic stable structures from core to shell but instead, due to phase separation behavior (Fig.2(c)) the delithiated core-shell materials would not thermodynamically form a gradual solid solution from core to shell. Hence, the compositions and stability of of concentration-gradient materials are strongly dependant on the nature of the phase diagrams.

Other phase regions of the quaternary system can be seen by considering two independent composition variable  $x$  and  $y$  simultaneously. Most of tie lines in the 0 K phase diagram develop into two phase regions as indicated by the shaded areas in Fig. 2(a). For the Mn-rich materials, a two phase region of  $\square\text{Mn}_2\text{O}_4$  and  $\text{LiMn}_{2-\delta}\text{Ni}_\delta\text{O}_4$  ( $0 \leq \delta \leq 0.1$ ) is formed, which corresponds to a tie line of  $\square\text{Mn}_2\text{O}_4$  and  $\text{LiMn}_2\text{O}_4$  at 0 K. Similarly, the two phase region of  $\square\text{Mn}_2\text{O}_4$  and  $\text{LiMn}_{1.5}\text{Ni}_{0.5}\text{O}_4$  has a corresponding tie line in Fig. 1(b). The region between these two phase regions is a three phase region including  $\square\text{Mn}_2\text{O}_4$ ,  $\text{LiMn}_{2-\delta}\text{Ni}_\delta\text{O}_4$  ( $0 \leq \delta \leq 0.1$ ) and  $\text{LiMn}_{1.5+\delta}\text{Ni}_{0.5-\delta}\text{O}_4$  ( $0.05 \leq \delta \leq 0.1$ ). Interestingly, the points of  $\text{LiMn}_{1.5}\text{Ni}_{0.5}\text{O}_4$  and  $\text{LiMnNiO}_4$  representing ordered ground states at 0 K grow into off-stoichiometric single phase regions around  $x = 1.5$  and  $x = 1$ , respectively. Other single phase regions derived from ordered ground states ( $\square\text{Mn}_2\text{O}_4$ ,  $\square\text{Ni}_2\text{O}_4$ , and  $\text{LiMn}_2\text{O}_4$ ) are very small at 300 K and thus appear just as points (line compounds).

Having established the binary and quaternary phase diagrams with cluster expansion effective interactions, we turn our attention to the voltages of concentration-gradient materials as a function of Li composition by grand canonical Monte Carlo (GCMC) simulations. By assuming the metal atom diffusion is much slower in (Mn,Ni) sublattice than Li diffusion in the (Li, $\square$ ) sublattice, we consider states in which the (Mn,Ni) sublattice is “frozen” (i.e. not equilibrated) in a given configuration, and we allow the Li/*Box* sublattice to equilibrate. In this way, we can investigate the relationship between Mn/Ni configuration and Li content,

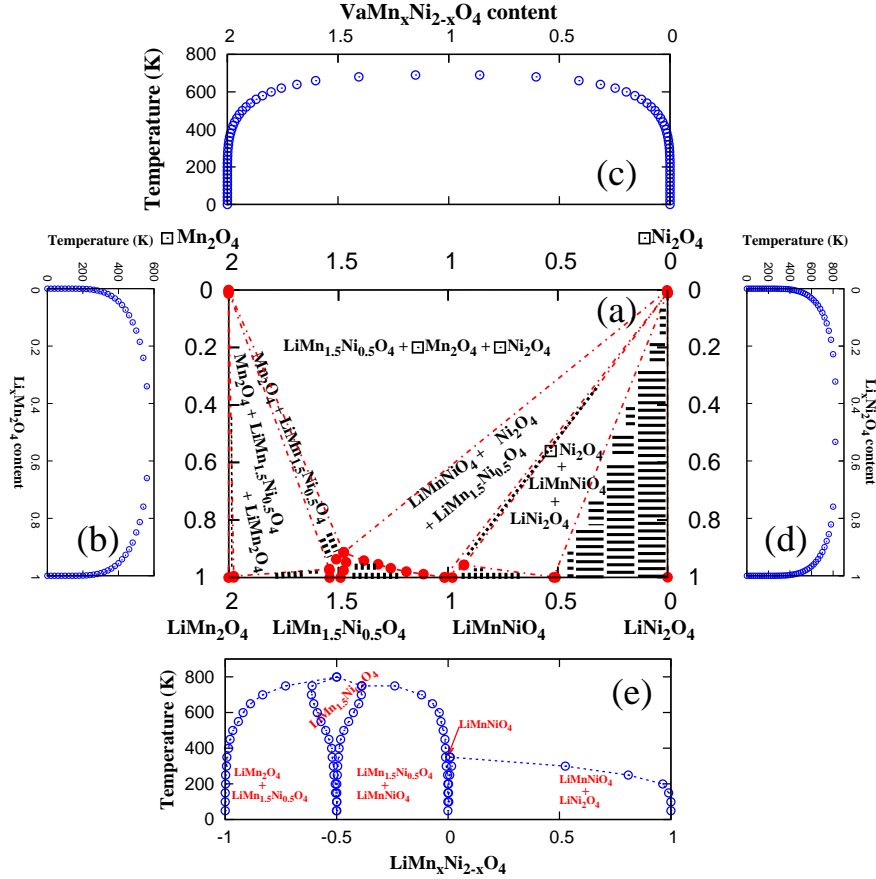


FIG. 2: Quaternary phase diagram of  $\text{Li}_y\text{□}_{1-y}\text{Mn}_x\text{Ni}_{2-x}\text{O}_4$  at 300 K with two phase region shaded (a) and corresponding binary phase diagrams of  $\text{Li}_y\text{Mn}_2\text{O}_4$  (b),  $\text{□Mn}_x\text{Ni}_{2-x}\text{O}_4$  (c),  $\text{Li}_y\text{Ni}_2\text{O}_4$  (d), and  $\text{LiMn}_x\text{Ni}_{2-x}\text{O}_4$  (e), respectively. The binary diagrams are computed as a function of temperature.

voltage, and temperature. We first use binary cluster interactions in the (Mn,Ni) sublattice with canonical Monte Carlo simulation to obtain the metal sublattice configurations. With the equilibrated metal sublattice configurations, we use GCMC simulation driven by the coupled cluster interactions to calculate voltages. The initial chemical potential of Li is calibrated the DFT voltage of spinel  $\text{LiMn}_2\text{O}_4$ .

Before we investigate the voltage of composite phases, we first discuss the voltages of single phases. We calculate voltage curves at 300 K for various (Mn, Ni) configurations of  $\text{LiMn}_x\text{Ni}_{2-x}\text{O}_4$  ( $x=2, 1.5, 1$ , and  $0$ ) by fixing the transition metal sublattice. For the four ordered single phases  $\text{LiMn}_2\text{O}_4$ ,  $\text{LiMn}_{1.5}\text{Ni}_{0.5}\text{O}_4$ ,  $\text{LiMnNiO}_4$ , and  $\text{LiNi}_2\text{O}_4$ , the voltage plateaus are 4.11, 4.65, 4.76, and 4.37 V respectively. These values are in good agreement with avail-

able experimental results of 4.1 V for  $\text{LiMn}_2\text{O}_4$  [38] and 4.7 V for  $\text{LiMn}_{1.5}\text{Ni}_{0.5}\text{O}_4$ . [39] To investigate the effects of long- and short-range order of metal atoms on the voltage of spinel structure, we calculate the voltage curves of  $\text{LiMn}_{1.5}\text{Ni}_{0.5}\text{O}_4$  and  $\text{LiMnNiO}_4$ , with different metal (Mn,Ni) configurations. As shown in Fig. 3(a), we consider three (Mn,Ni) configurations including (a) perfect (T=0 K) (Mn,Ni) ordered configurations, (b) equilibrated (Mn,Ni) configurations at 300 K by Monte Carlo, and (c) completely random (Mn,Ni) sublattice (high temperature). For each case, the (Mn,Ni) sublattices are fixed, and the (Li, $\square$ ) sublattice is allowed to equilibrate. We find that disorder on the metal sublattice results in a voltage decrease for both  $\text{LiMn}_{1.5}\text{Ni}_{0.5}\text{O}_4$  and  $\text{LiMnNiO}_4$ . For the completely random (Mn,Ni) configurations, the voltage does not decrease as plateau, but continuously as the Li content increases. It is worth mentioning that we didn't get a tiny voltage step for  $\text{Li}_x\text{Mn}_{1.75}\text{Ni}_{0.25}\text{O}_4$  with disordered ( $\text{Fd}\bar{3}\text{m}$ ) Mn/Ni configuration as experimental suggested. [40] Our calculation results are also different from previous calculations, where the Li-vacancy ordering with disordered Mn/Ni sublattice is found favorable relative to (de)lithiated states. [41, 42] The difference is rooted in our choice of ferromagnetic states for fully (de)lithiated states as references, while previous work took ferrimagnetic (for fully lithiated) and extrapolated energy (for fully delithiated) as references.[41]

We also calculate the voltage of composite, two phase mixtures, specifically  $\text{LiMn}_x\text{Ni}_{2-x}\text{O}_4$  at compositions ( $x=1.75, 1.25, 0.5$ ). According to the binary phase diagram as shown in Fig.2(e),  $\text{LiMn}_x\text{Ni}_{2-x}\text{O}_4$  ( $x=1.75, 1.25, 0.5$ ) will decompose into two phases at low temperatures. For example,  $\text{LiMn}_{1.75}\text{Ni}_{0.25}\text{O}_4$  will decompose into  $\text{LiMn}_2\text{O}_4$  and  $\text{LiMn}_{1.5}\text{Ni}_{0.5}\text{O}_4$ . Thus the  $\text{LiMn}_x\text{Ni}_{2-x}\text{O}_4$  ( $x=1.75, 1.25, 0.5$ ) can be viewed as composite cathode materials. For these composite cathodes, we first perform canonical Monte Carlo simulations to equilibrate the metal sublattice while keeping the Li sublattice frozen. After equilibration of the metal sublattice, the metal sites are frozen and we use GCMC to investigate Li voltage as a function of Li content. The voltages of composite two phase materials are shown in Fig.3(b). Clearly, there are two voltage plateaus for all three compositions. For example, the first plateau of  $\text{LiMn}_{1.75}\text{Ni}_{0.25}\text{O}_4$  ( $=\text{LiMn}_{1.5}\text{Ni}_{0.5}\text{O}_4 + \text{LiMn}_2\text{O}_4$ ) is around 4.58 V, which is a little lower than  $\text{LiMn}_{1.5}\text{Ni}_{0.5}\text{O}_4$  at 300 K, while the second plateau is around 4.1 V, which is close to the voltage of  $\text{LiMn}_2\text{O}_4$ . Similarly, the two plateaus of  $\text{LiMn}_{1.25}\text{Ni}_{0.75}\text{O}_4$  correspond to  $\text{LiMnNiO}_4$  and  $\text{LiMn}_{1.5}\text{Ni}_{0.5}\text{O}_4$ , respectively. It is reasonable to see that the voltage changes from one plateau to the other around 50% Li because the compositions

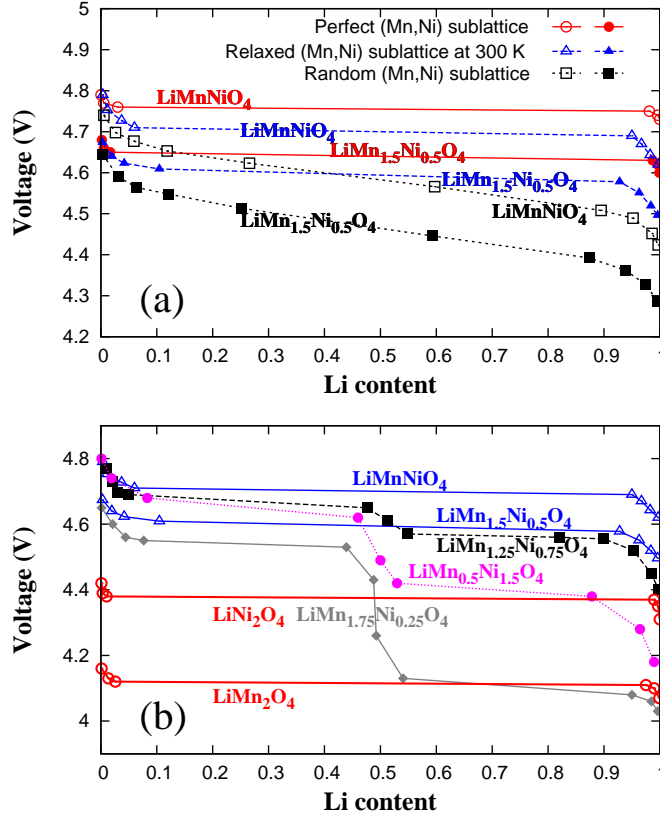


FIG. 3: Calculated voltages of (a)  $\text{LiMnNiO}_4$  (open symbols) and  $\text{LiMn}_{1.5}\text{Ni}_{0.5}\text{O}_4$  (solid symbols) for various configurations of the (Mn,Ni) sublattice, and (b) comparison of voltages from single phases of  $\text{LiMn}_x\text{Ni}_{2-x}\text{O}_4$  ( $x=2, 1.5, 1,$  and  $0$ ) with composite phases of  $\text{LiMn}_x\text{Ni}_{2-x}\text{O}_4$  ( $x=1.75, 1.25,$  and  $0.5$ ).

chosen have approximately equal amounts of decomposed products, e.g.  $\text{LiMn}_{1.75}\text{Ni}_{0.25}\text{O}_4 \rightarrow 0.5*\text{LiMn}_2\text{O}_4+0.5*\text{LiMn}_{1.5}\text{Ni}_{0.5}\text{O}_4$  and  $\text{LiMn}_{0.5}\text{Ni}_{1.5}\text{O}_4 \rightarrow 0.5*\text{LiMnNiO}_4+0.5*\text{LiNi}_2\text{O}_4$ . From the voltage profiles, it is can be seen that during discharge Li always initially intercalates in the high voltage (low chemical potential) phase, and then the low voltage phase. Thus, if there are equal amounts of two phases in the composite cathode material, the voltage will significantly shift from one plateau to the other around 50% Li as shown in Fig.3(b). On the other hand, if we tune the ratio of two phases by adjusting Mn/Ni composition, the corresponding voltage plateaus will also change. For example, for  $\text{LiMn}_{1.9}\text{Ni}_{0.1}\text{O}_4 \rightarrow 0.8*\text{LiMn}_2\text{O}_4+0.2*\text{LiMn}_{1.5}\text{Ni}_{0.5}\text{O}_4$ , the voltage would significantly change around 20% Li. Thus, for a core-shell type concentration-gradient material with spinel  $\text{LiMn}_2\text{O}_4$  core and spinel  $\text{LiNi}_2\text{O}_4$  shell, the composite voltage profile would be dominated by four voltage

plateaus of intermediate structures dropping down in an order of  $\text{LiMnNiO}_4$ ,  $\text{LiMn}_{1.5}\text{Ni}_{0.5}\text{O}_4$ ,  $\text{LiNi}_2\text{O}_4$ , and  $\text{LiMn}_2\text{O}_4$ . On the basis of the voltages of single phase and composites, the desired voltage profile of concentration gradient particles can be achieved by tailoring the composition of Mn or Ni concentration.

#### IV. CONCLUSIONS

In summary, we systematically studied the thermodynamics of ordering and phase-separation in the quaternary  $\text{Li}_y\text{Mn}_x\text{Ni}_{2-x}\text{O}_4$  system by DFT calculations together with cluster expansion methods and Monte Carlo simulations. Isothermal section of the quaternary phase diagram are constructed at  $T=0$  and 300 K. We predict two ordered quaternary spinel phases: the well-known  $\text{LiMn}_{1.5}\text{Ni}_{0.5}\text{O}_4$  phase and a new as-yet unobserved  $\text{LiMnNiO}_4$  phase. The  $\text{LiMnNiO}_4$  phase has a very high predicted voltage of 4.76 V. GCMC simulations on the voltages of  $\text{LiMnNiO}_4$  and  $\text{LiMn}_{1.5}\text{Ni}_{0.5}\text{O}_4$  suggest that disorder of the metal (Mn,Ni) sublattice results in a voltage decrease. For the composite two phase cathode materials, the voltages show combinations of plateaus from each phase. The quaternary phase diagram and voltage calculations are help guide our understanding and design of concentration gradient material with target voltage profiles.

#### Acknowledgments

The authors acknowledge support from The Dow Chemical Company. The initial stages of this work was supported by the Center for Electrochemical Energy Science (CEES), an Energy Frontier Research Center (EFRC) funded by the U.S. Department of Energy, Office of Science, Office of Basic Energy Sciences (Award No. DE-AC0206CH11357). High performance computational resources from the Northwestern University are acknowledged.

- 
- [1] M. Armand and J. M. Tarascon, *Nature* **451**, 652 (2008).
  - [2] A. S. Arico, P. Bruce, B. Scrosati, J. M. Tarascon, and W. Van Schalkwijk, *Nat. Mater.* **4**, 366 (2005).
  - [3] M. M. Thackeray, C. Wolverton, and E. D. Isaacs, *Energy & Environ. Sci.* **5**, 7854 (2012).

- [4] H. Li, Z. Wang, L. Chen, and X. Huang, *Adv. Mater.* **21**, 4593 (2009).
- [5] L. Su, Y. Jing, and Z. Zhou, *Nanoscale* **3**, 3967 (2011).
- [6] H. Li and H. Zhou, *Chem. Commun.* **48**, 1201 (2012).
- [7] Y. M. Lin, H. C. Wu, Y. C. Yen, Z. Z. Guo, M. H. Yang, H. M. Chen, H. S. Sheu, and N. L. Wu, *J. Electrochem. Soc.* **152**, A1526 (2005).
- [8] J. Cho, H. Kim, and B. Park, *J. Electrochem. Soc.* **151**, A1707 (2004).
- [9] Y. K. Sun, M. J. Lee, C. S. Yoon, J. Hassoun, K. Amine, and B. Scrosati, *Adv. Mater.* **24**, 1192 (2012).
- [10] S. T. Myung, K. S. Lee, C. S. Yoon, Y. K. Sun, K. Amine, and H. Yashiro, *J. Phys. Chem. C*, **114**, 4710 (2010).
- [11] M. Aykol, S. Kirklin, and C. Wolverton, *Adv. Energ. Mater.* **4**, 1400690 (2014).
- [12] S. Hao and C. Wolverton, *J. Phys. Chem. C* **117**, 8009 (2013).
- [13] Y. K. Sun, S. T. Myung, M. H. Kim, J. Prakash, and K. Amine, *J. Am. Chem. Soc.* **127**, 13411 (2005).
- [14] Y. K. Sun, S. T. Myung, B. C. Park, J. Prakash, I. Belharouak, and K. Amine, *Nat. Mater.* **8**, 320 (2009).
- [15] Y. K. Sun, Z. Chen, H. J. Noh, D. J. Lee, H. G. Jung, Y. Ren, S. Wang, Y. C. S., S. T. Myung, and K. Amine, *Nat. Mater.* **11**, 942 (2012).
- [16] J. M. Sanchez, F. Ducastelle, and G. Gratias, *Physica A* **128**, 334 (1984).
- [17] P. Tepeš, G. D. Garbulsky, and G. Ceder, *Phys. Rev. Lett.* **74**, 2272 (1995).
- [18] P. E. Blöchl, *Phys. Rev. B* **50**, 17953 (1994).
- [19] J. P. Perdew, K. Burke, and M. Ernzerhof, *Phys. Rev. Lett.* **77**, 3865 (1996).
- [20] S. L. Dudarev, G. A. Botton, S. Y. Savrasov, C. J. Humphreys, and A. P. Sutton, *Phys. Rev. B* **57**, 1505 (1998).
- [21] G. Kresse and J. Furthmüller, *Phys. Rev. B* **54**, 11169 (1996).
- [22] F. Zhou, M. Cococcioni, C. A. Marianetti, D. Morgan, and G. Ceder, *Phys. Rev. B* **70**, 235121 (2004).
- [23] A. van de Walle, M. Asta, and G. Ceder, *CALPHAD Journal* **26**, 539 (2002).
- [24] A. van de Walle and M. Asta, *Modelling Simul. Mater. Sci. Eng.* **10**, 521 (2002).
- [25] K. Amine, H. Tukamoto, H. Yasuda, and Y. Fujita, *J. Power Sour.* **68**, 604 (1997).
- [26] J. Bhattacharya and C. Wolverton, *J. Electrochem. Soc.* **161**, A1440 (2014).

- [27] H. Berg, J. O. Thomas, L. Wen, and G. C. Farrington, *Solid State Ionics* **112**, 165 (1998).
- [28] J. Cabana, M. Casas Cabanas, F. O. Omenya, N. A. Chernova, Z. Dongli, M. S. Whittingham, and C. P. Grey, *Chem. Mater.* **24**, 2952 (2012).
- [29] J. Song, D. W. Shin, Y. Lu, C. D. Amos, A. Manthiram, and J. B. Goodenough, *Chem. Mater.* **24**, 3101 (2012).
- [30] J.-H. Kim, A. Huq, M. Chi, N. P. W. Pieczonka, E. Lee, C. A. Bridges, M. M. Tessema, A. Manthiram, K. A. Persson, and B. R. Powell, *Chem. Mater.* **26**, 4377 (2014).
- [31] A. Sagua, G. M. Lescano, J. A. Alonso, R. Martinez-Coronado, M. T. Fernandez-Diaz, and E. Moran, *Materials Research Bulletin* **47**, 1335 (2012).
- [32] C. A. Barrett and E. B. Evans, *J. Am. Ceram. Soc.* **47**, 533 (1964).
- [33] H. Taguchi, S. Omori, M. Nagao, H. Kido, and M. Shimada, *J. Solid State Chem.* **118**, 112 (1995).
- [34] A. Van der Ven, C. Marianetti, D. Morgan, and G. Ceder, *Solid State Ionics* **135**, 21 (2000).
- [35] L. Wang, T. Maxisch, and G. Ceder, *Chem. Mater.* **19**, 543 (2007).
- [36] R. J. Gummow and M. M. Thackeray, *J. Electrochem. Soc.* **141** (1994).
- [37] W. Liu, K. Kowal, and G. C. Farrington, *J. Electrochem. Soc.* **145**, 459 (1998).
- [38] J. M. Tarascon, E. Wang, F. K. Shokoohi, W. R. McKinnon, and S. Colson, *J. Electrochem. Soc.* **138**, 2859 (1991).
- [39] Q. M. Zhang, A. Bonakdarpour, Y. Zhang M. J. Gao, and J. R. Dahn, *J. Electrochem. Soc.* **144**, 205 (1997).
- [40] J. H. Kim, S. T. Myung, C. S. Yoon, S. G. Kang, and Y. K. Sun, *Chem. Mater.* **16**, 906 (2004).
- [41] E. Lee and K. A. Persson, *Energy & Environ. Sci.* **5**, 6047 (2012).
- [42] E. Lee and K. A. Persson, *Chem. Mater.* **25**, 2885 (2013).